Composites: Part A xxx (2011) xxx–xxx

Contents lists available at SciVerse ScienceDirect

Composites: Part A

journal homepage: www.elsevier.com/locate/compositesa

Interlaminar fracture analysis in the G_{II}–G_{III} plane using prestressed transparent composite beams

András Szekrényes *, William Martins Vicente

Budapest University of Technology and Economics, Department of Applied Mechanics, Müegyetem rkp. 5, 1111 Budapest, Building MM, Hungary

ARTICLE INFO

Article history:
Received 29 May 2011
Received in revised form 19 August 2011
Accepted 18 September 2011
Available online xxxx

Keywords:
A. Glass fibers
B. Delamination
C. Finite element analysis (FEA)
D. Mechanical testing

ABSTRACT

This work presents the mixed-mode II/III prestressed split-cantilever beam specimen for the fracture testing of composite materials. In accordance with the concept of prestressed composite beams one of the two fracture modes is provided by the prestressed state of the specimen, and the other one is increased up to fracture initiation by using a testing machine. The novel beam-like specimen is able to provide any combinations of the mode-II and mode-III ERRs. Data reduction is made by using the virtual crack-closure technique. The applicability and the limitations of the novel fracture mechanical test are demonstrated using unidirectional glass/polyester composite specimens. If only crack propagation onset is involved then the mixed-mode beam specimen can be used to obtain the fracture criterion of transparent composite materials in the G_{II}–G_{III} plane in a relatively simple way.

1. Introduction

The investigation of the interlaminar fracture toughness of composite materials is important due to their susceptibility to delamination caused by, e.g., low-velocity impact, edge effect or combined mechanical load. For mode-I and mode-II there are standard methods to help the design of composite structures with cracks and notches [1,2]. The international standards (ASTM, ESIS) propose also fracture tests for the mixed-mode I/II cases [3,4]. There is a quite different status considering the mode-III fracture of composites. Based on the state-of-art review of the present situation the following systems are available for mode-III delamination testing:

- the crack rail shear test (CRS) [5],
- the split-cantilever beam (SCB) [6],
- the edge-crack torsion (ECT) test [7–11],
- the modified version of the split-cantilever beam [12–15],
- the anticlastic plate bending (APCB) method [16],
- the mode-III four point-bend end-notched flexure (4ENF$_{III}$) [17],
- the four-point bending plate test (4PBP) [18],
- the updated version of the modified split-cantilever beam [19],
- the 6-point edge crack torsion (6ECT) [20],
- the shear-torsion-bending (STB) test [21].

This short review shows that the development of mode-III fracture tools is still in progress. The main reason for that is each system is useful and – more or less – works fine, in spite of that there are also significant drawbacks compared to the relatively simple mode-I and mode-II tests. Among others, the complex fixtures, the difficult data reduction and specimen preparation (mainly in plate specimens) can be mentioned. When a mode-III system is to be chosen, one of the aspects can be whether the system can be extended for mixed-mode I/III, II/III and I/II/III conditions or not. In this respect the composite literature offers the following mixed-mode configurations:

- the prestressed end-notched flexure (PENF$_{II/III}$) [22],
- the 8-point bending plate (8PBP, mixed-mode I/III) system [23],
- the 6-point bending plate (6PBP, mixed-mode II/III) system [24],
- the prestressed split-cantilever beam (PSCB$_{I/III}$) [25],
- the double-notched split cantilever beam (DNSCB, mixed-mode II/III) [26],
- the shear-torsion-bending test (STB) [21].

In the case of the PENF$_{II/III}$ and PSCB$_{I/III}$ systems beam-like specimens are used, and one of the energy release rates (ERR) is prestressed providing a fixed value, while the other component is increased up to fracture initiation. The advantages are that there is an analytical reduction technique, the specimen geometry is simple and both uni- and multidirectional lay-up can be applied, however the drawbacks are that the mode ratio changes along the crack front, with the crack length and applied load [25]. The 6PBP and 8PBP systems apply cross-ply laminated plates subjected to bending and because of that specimen preparation requires

* Corresponding author.
E-mail addresses: szeki@mm.bme.hu (A. Szekrényes), williamefei@gmail.com (W.M. Vicente).
URL: http://www.mm.bme.hu/~szeki (A. Szekrényes).

1359-835X/$ - see front matter © 2011 Elsevier Ltd. All rights reserved.
doi:10.1016/j.compositesa.2011.09.022

much effort [23,24]. Moreover the data reduction is possible only by a finite element (FE) model including virtual crack-closure technique (VCCT) and cohesive zone model (CZM) applications. The DNSCB test eliminates the torsion in the SCB test by applying a double-notched beam with applied loads parallel to the delamination plane [26]. In the DNSCB system it is not possible to vary the mode ratio. The newest development is the STB test [21], which is a promising method, although the extension of the fixture for mode II/III and mode I/II/III fracture is still in progress. Otherwise the STB maintains the complex fixture, and requires specimens with edge delaminations. This short introduction shows that this field of fracture mechanics is not sufficiently mapped, and that we need more information on how the composite materials behave under the presence of the mode-III ERR.

This work is intended to develop a novel mixed-mode II/III fracture test. The original concept of prestressed composite beams was applied first for mixed-mode I/II [27], later it was extended to II/III [22] and I/III [25] cases. Although the $PENF_{II/III}$ [22] worked, the crack length was restricted by the central load introductor of the three-point bending setup, on the other hand the mode-III ERR (ERR) was initially prestressed. Due to the low compliance of the MSCB system it is more reasonable to prestress the mode-II part and measure the mode-III ERR. In the present work we introduce the mixed-mode II/III version of the PSCB system. FE analysis is conducted to show the distribution of the ERR during the fracture process. It is assumed that crack initiation takes place at the point where the highest ERR is available. Finally, the fracture envelope in the G_{II}–G_{III} plane is constructed and compared to those created in the G_I-G_{II} and G_I–G_{III} planes based on previous works.

2. The PSCB specimen for mixed-mode II/III cracking

The $PSCB_{II/III}$ specimen is the combination of the end-loaded split (ELS) and MSCB specimens [19]. Fig. 1 shows the 3D model of the system developed in SOLIDWORKS. The MSCB part is identical to that presented in previous papers [19,28]. We note that the present MSCB fixture allows the rotation of the specimen end about the x axis. Prevention of the rotation is possible only by very stiff steel rigs, which leads to significant frictional effects [13,29,14]. To produce mixed-mode II/III condition the specimen is put into a prestresser given by Fig. 2. The exploded view shows that the notched shaft (No. 5) is constrained by ball and roller bearings, therefore the specimen is free to rotation about the x axis and its end is fixed, as it is shown by the second figure. Eventually, by fixing the transverse (y) displacement the mode-II ERR can be set through an ELS configuration. The specimen together with the prestresser is put between the rigs of the MSCB system. In Fig. 1 No. 8 refers to the prestresser. In the sequel we treat the system as the superposition of the ELS and MSCB systems shown in Fig. 3. According to Fig. 3 the load P_{ELS} is related to the mode-II part of the ERR, while P_1 and P_2 are the loads related to the mode-III loading. Based on the equilibrium of the system we have: $P_1 = P_{MSCB} \cdot s_2/s_1$ and $P_2 = P_{MSCB} \cdot (1 + s_2/s_1)$, where P_{MSCB} is the load transferred through roller C, s_1 and s_2 are the distances between rollers A, B and C (see Fig. 4). Fig. 4 shows the 2D views of the prestressed specimen and the loading grips. The mode-II part of the ERR is fixed by the prestresser nut.

The MSCB loading rigs transfer a scissor-like load to the prestressed specimen through rollers A and B. The external load, P_{MSCB} is introduced through roller C by a testing machine. To ensure the position of rollers A and B along the thickness of the specimen, they were substituted by grub screws, which can be adjusted by using a screwdriver. The grub screws run over the prestresser tool, and at the end of the screws small disks were attached. By the proper adjustment of the axial position of the screws it is possible to realize that the disks belonging to the same grip have almost the same axial (y) position with respect to the x–z plane. This involves the rotation of the prestresser block about the z axis, as it is shown by the top view in Fig. 4. The moment equilibrium of the system about the x axis is ensured by the shaft and the hub of the load transfer plate (refer to Fig. 1). Essentially, we apply the VCCT for data reduction, however, to verify the load displacement-slopes and the linear elastic behavior of the system the compliance of the MSCB system was utilized.

3. Analysis

The analysis of the MSCB specimen is detailed in [19]. The improved beam theory (IBT) model takes four mechanical deformations into account: bending and shearing of the specimen arms, the Saint–Venant effect at the crack front and the free torsion effect in the delaminated portion. The compliance and the ERR calculated by the analytical solution were compared to the results of a three-dimensional FE model and an excellent agreement was found.

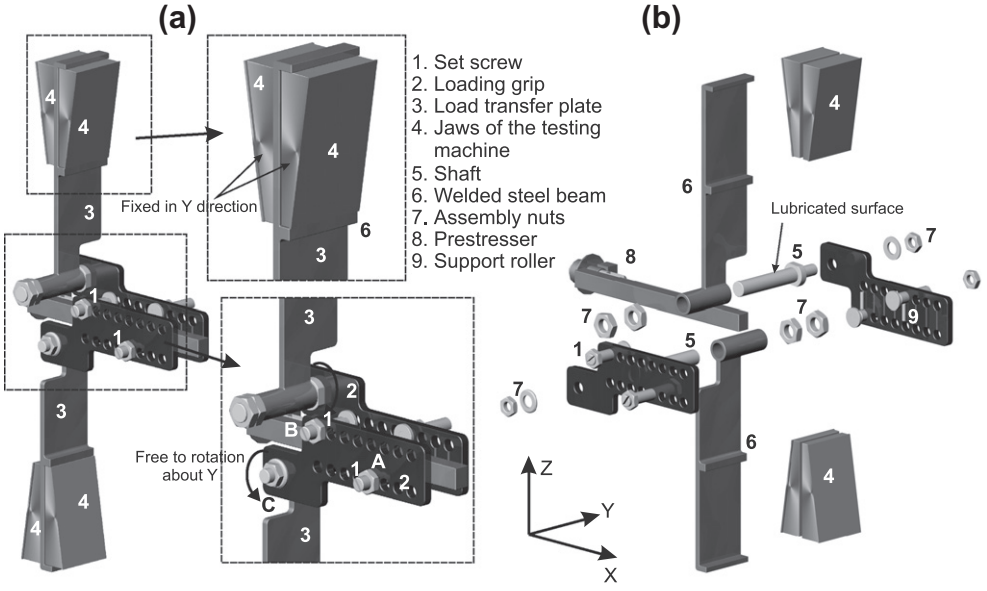

Fig. 1. The 3D views of the $PSCB_{II/III}$ specimen, assembled state (a), exploded view (b).

Please cite this article in press as: Szekrényes A, Vicente WM. Interlaminar fracture analysis in the G_{II}–G_{III} plane using prestressed transparent composite beams. Composites: Part A (2011), doi:10.1016/j.compositesa.2011.09.022

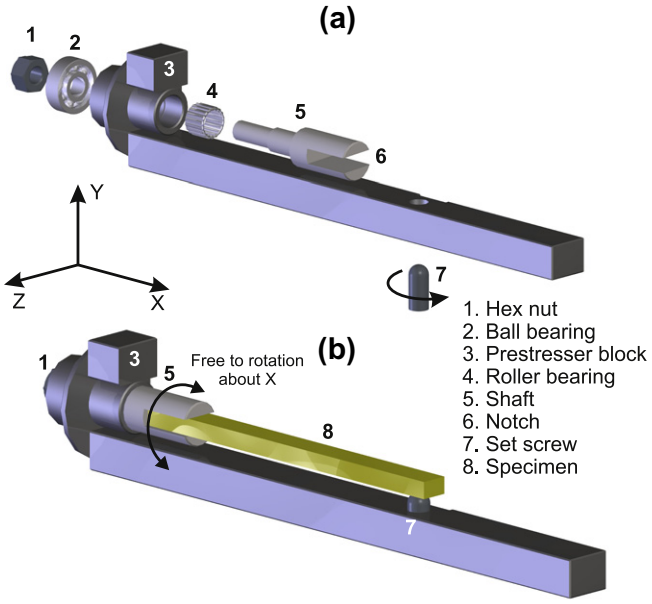

Fig. 2. Prestresser for the $PSCB_{II/III}$ test, exploded view (a), assembled state (b). (For interpretation of the references to colour in this figure legend, the reader is referred to the web version of this article.)

Since the MSCB specimen is loaded at four points it should be mentioned that the compliance is calculated at the point of external load application, i.e. at roller C in Fig. 4, apparently, the compliance can be measured only at this point, which is:

$$C_{MSCB} = \frac{8a^3}{b^3 h E_{11}}\left[f_{EB1}^{MSCB} + f_{TIM1}^{MSCB} + f_{FT1}^{MSCB} + f_{S-V1}^{MSCB}\right], \tag{1}$$

where a is the crack length, b is the specimen width, h is the half thickness, E_{11} is the flexural modulus of the material. The terms in the brackets consider bending, transverse shear, free torsion and Saint–Venant effects:

$$f_{EB1}^{MSCB} = 1 - 3\left(\frac{s_1+s_2}{a}\right) + 3\left(\frac{s_1+s_2}{a}\right)^2 - \frac{s_1(s_1+s_2)(s_1+2s_2)}{a^3} \tag{2}$$

$$f_{TIM1}^{MSCB} = 0.3\left(1 - \frac{s_2^2 - s_1^2}{a s_1}\right)\left(\frac{b}{a}\right)^2\left(\frac{E_{11}}{G_{13}}\right) \tag{3}$$

$$f_{FT1}^{MSCB} = 0.19\frac{1}{\varsigma}\left(1 - \frac{s_1}{a}\right)\left(\frac{b}{a}\right)^2\left(\frac{E_{11}}{G_{12}}\right) \tag{4}$$

$$f_{S-V1}^{MSCB} = 0.48\left(\frac{a-(s_1+s_2)}{a}\right)^2\left(\frac{b}{a}\right)\left(\frac{E_{11}}{G_{13}}\right)^{\frac{1}{2}} \tag{5}$$

and:

$$\varsigma = 1 - 0.63\mu\frac{h}{b}, \mu = \left(\frac{G_{13}}{G_{12}}\right)^{\frac{1}{2}} \tag{6}$$

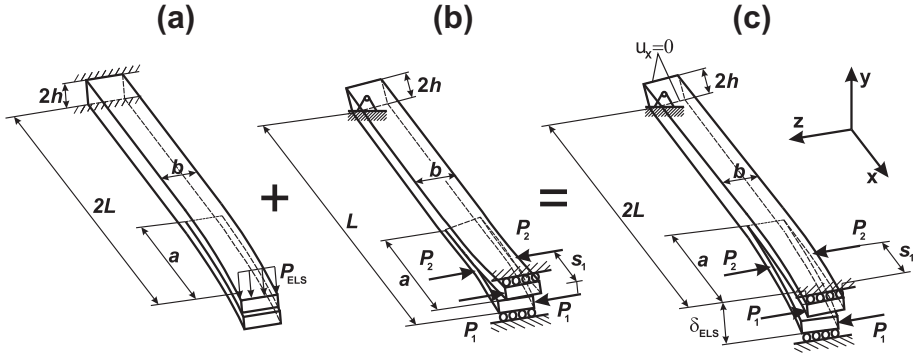

Fig. 3. The $PSCB_{II/III}$ specimen (c) as the superposition of the ELS (a) and MSCB (b) systems.

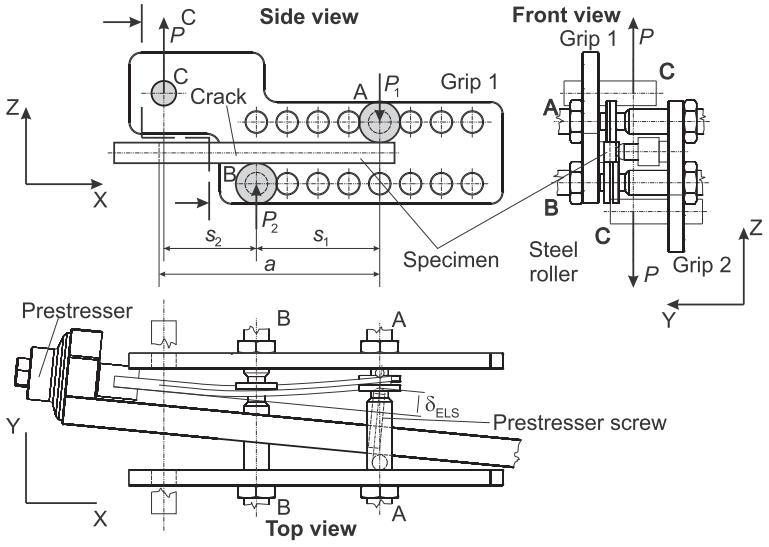

Fig. 4. The side, front and top views of the $PSCB_{II/III}$ system.

Please cite this article in press as: Szekrényes A, Vicente WM. Interlaminar fracture analysis in the G_{II}–G_{III} plane using prestressed transparent composite beams. Composites: Part A (2011), doi:10.1016/j.compositesa.2011.09.022

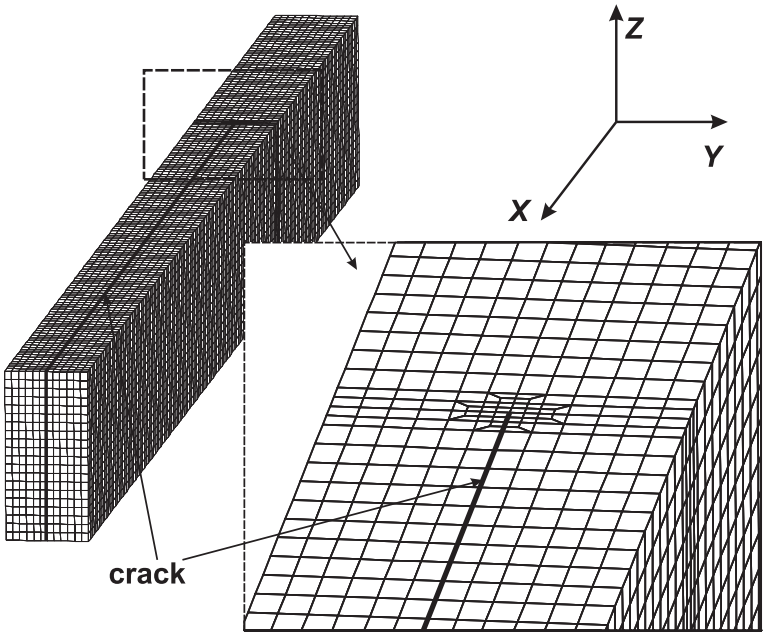

Fig. 5. The ANSYS finite element model of the $PSCB_{II/III}$ system.

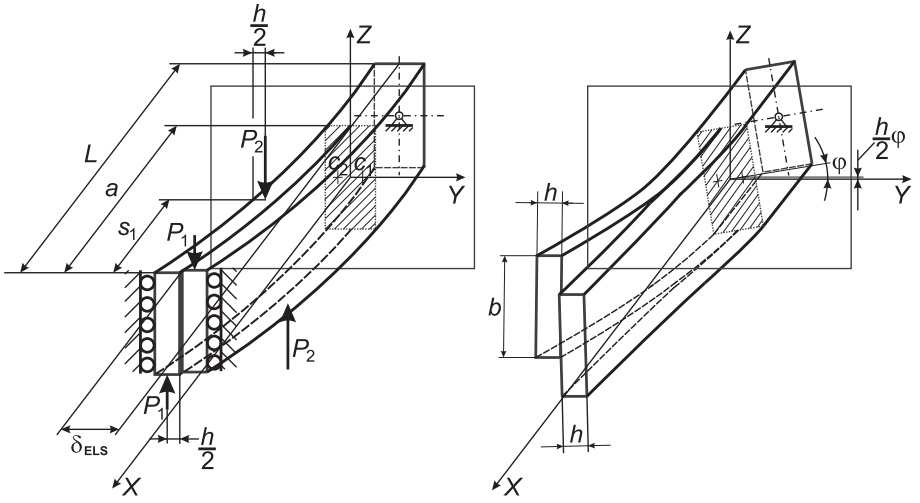

Fig. 6. The applied kinematic and dynamic boundary conditions in the finite element model of the $PSCB_{II/III}$ specimen.

where G_{12} and G_{13} are the shear moduli in the x–y and x–z planes, respectively s_1 and s_2 are the distances between the loading rollers A, B and C, respectively (see Fig. 4). Although the ERR can be calculated based on the former equations, this results in the widthwise average ERR. The $PMSCB_{II/III}$ produces non-uniform ERR distribution, therefore for the ERR the analytical model can not be used. Also, it has been shown that the condition of at least a 96% mode-III dominant test is [19]:

$$1.02 \leqslant a/(s_1 + s_2) \leqslant 1.09 \tag{7}$$

3.1. The dependence of the mode ratio on the system parameters

The accurate measurement of the crack length after crack initiation is important. During the experiments (see later) a transparent material is used, accordingly the crack initiation is easy to identify visually.

In practice, the displacement is set by a screwdriver and it can be assumed that the accuracy of the human eye is about ± 0.25 mm in the course of the adjustment of the prestress displacement δ_{ELS}. The most critical point in this respect is that first we have to touch the surface of the specimen, this point is thought to be the origin in the load–displacement response. Then, by knowing the pitch of the grub screw (see Fig. 2a) it is possible to set the displacement value by the number of revolutions. The mode ratio is influenced by this effect, but apart from that G_{II}/G_{III} depends also on P_{MSCB}.

A major question in a mixed-mode configuration is how the mode ratio changes along the crack front. To clarify this question a 3D FE model shown by Fig. 5 in the ANSYS 12 package was used [25]. The elastic properties of the models were: E_{11} = 33 GPa, $E_{22} = E_{33}$ = 7.2 GPa, $G_{12} = G_{13} = G_{23}$ = 3 GPa and $\nu_{12} = \nu_{13} = \nu_{23}$ = 0.27. The geometric properties were: b = 12.8 mm, $2h$ = 6.2 mm, s_1 = 57.38 mm, s_2 = 49.36 mm and the length of the models was L = 118 mm (refer to Fig. 1). We note that s_1 and s_2 were calculated based on [30]. The imposed boundary conditions and the loading of the model are demonstrated in Fig. 6. First, the model was loaded at the end of the specimen arm by a displacement value equal to δ_{ELS} = 4.6875, 6.25, 8.125, 9.375, 10.625 and 11.875 mm providing the mode-II part of the

Please cite this article in press as: Szekrényes A, Vicente WM. Interlaminar fracture analysis in the G_{II}–G_{III} plane using prestressed transparent composite beams. Composites: Part A (2011), doi:10.1016/j.compositesa.2011.09.022

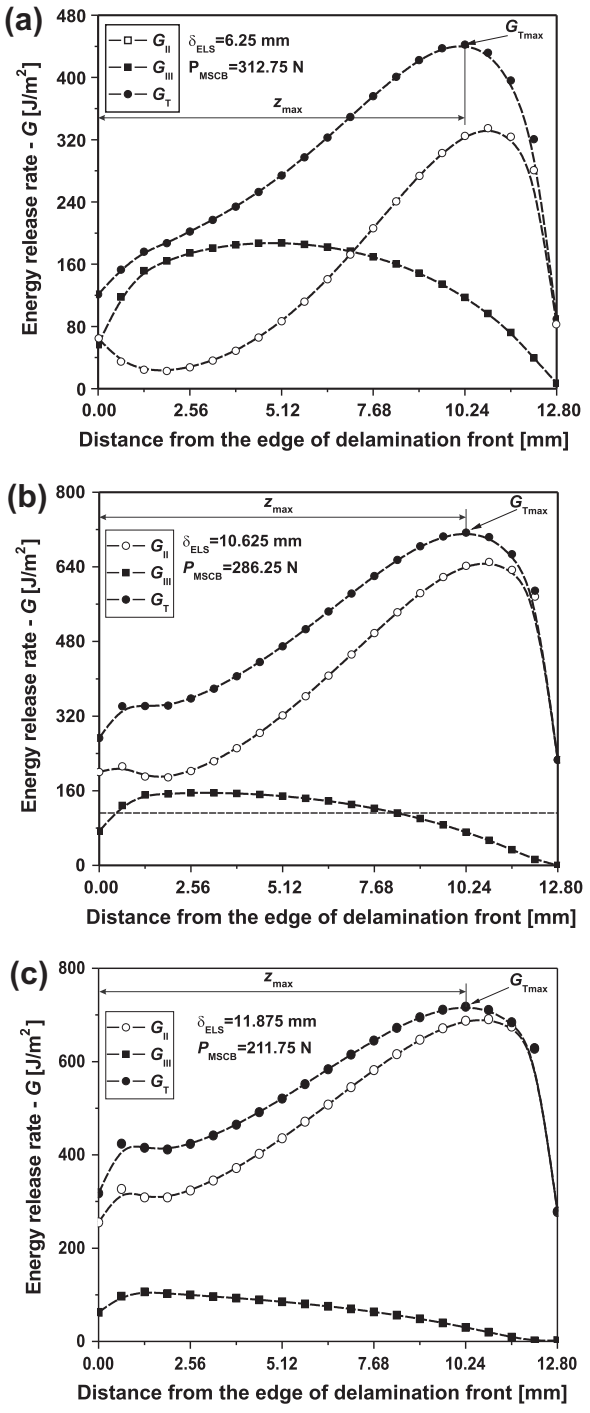

Fig. 7. The distribution of the mode-II, mode-III and total energy release rates along the specimen width.

mixed-mode II/III ERR. These values were calculated from the number of revolutions and the pitch (1.25 mm) of the prestressing screw. On the other hand the model was also loaded in two planes parallel to the delamination (from $h/2$ distance to the specimen side) applying the load values (P_1 and P_2) which were calculated using the experimentally measured P_{MSCB} loads based on crack initiation tests ($P_1 = P_{MSCB} \cdot s_2/s_1$ and $P_2 = P_{MSCB} \cdot (1 + s_2/s_1)$). The ERRs were evaluated by using the VCCT [11,18], the size of the crack tip elements were $\Delta x = \Delta y = 0.25$ mm and $\Delta z = 0.64$ mm. Fig. 7 shows the distribution of the ERRs along the crack front in the case of $\delta_{ELS} = 6.25$, 10.625 and 11.875 mm. Based on the figures we can see that the

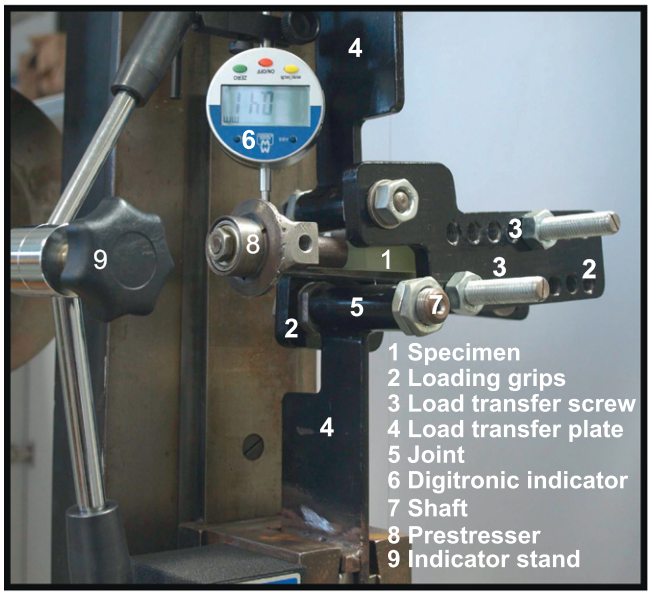

Fig. 8. The experimental equipment of the $PSCB_{II/III}$ system. (For interpretation of the references to colour in this figure legend, the reader is referred to the web version of this article.)

mode ratio G_{II}/G_{III} changes significantly over the specimen width. As it can be seen both the mode-II and mode-III ERRs have an asymmetric distribution along the crack front.

In our case $s_1 + s_2 = 57.38 + 49.36 = 106.74$ mm, which violates Eq. (7). That is because the position of the loading screws was fixed, and due to the given specimen width we were not able to choose better positions for s_1 and s_2.

Since the ERR varies along the crack front the specimen possessed a curved crack front under crack propagation. Accordingly, as it is seen in Fig. 6 a constant mode ratio along the crack front is not possible to be produced.

3.2. Point of crack initiation

In the data reduction and calculation of G_C and G_{II}/G_{III} it was assumed that the crack initiation takes place at the point where the highest total ERR ($G_T = G_{II} + G_{III}$) is available.

This assumption will be validated later by experiments. It must be noted that the pointwise detection of crack initiation does not consider a significant volume of material, which is important for obtaining representative properties in heterogeneous materials. However, for mode-III testing this is a significant difficulty. Based on the state-of-the-art larger volume in general involves larger specimen dimensions, more than one crack initiation points [18,23,24] and nonlinear response [9,21]. The material volume considered in the $PSCB_{II/III}$ is relatively small, which is a drawback. On the other hand the crack initiation can be detected accurately for transparent materials and the load–displacement response is linear.

The $PSCB_{I/II/III}$ involves several disadvantages. In fact the prestress can be relaxed during the test, which may cause considerable errors. Although in this work the point of crack initiation took place approximately at the highest G_T point, it is possible that the delamination does not start at this point. Moreover, the initiation energy release rate strongly depends on the initial crack tip condition, e.g., [31]. This effect was not considered here. In general, the energy release rate of steady crack propagation is a more reasonable value for discussing the interlaminar toughness of composite materials. Due to the variation of the mode ratio with the crack length the $PSCB_{I/II/III}$ is suitable only to perform initiation tests.

Please cite this article in press as: Szekrényes A, Vicente WM. Interlaminar fracture analysis in the G_{II}–G_{III} plane using prestressed transparent composite beams. Composites: Part A (2011), doi:10.1016/j.compositesa.2011.09.022

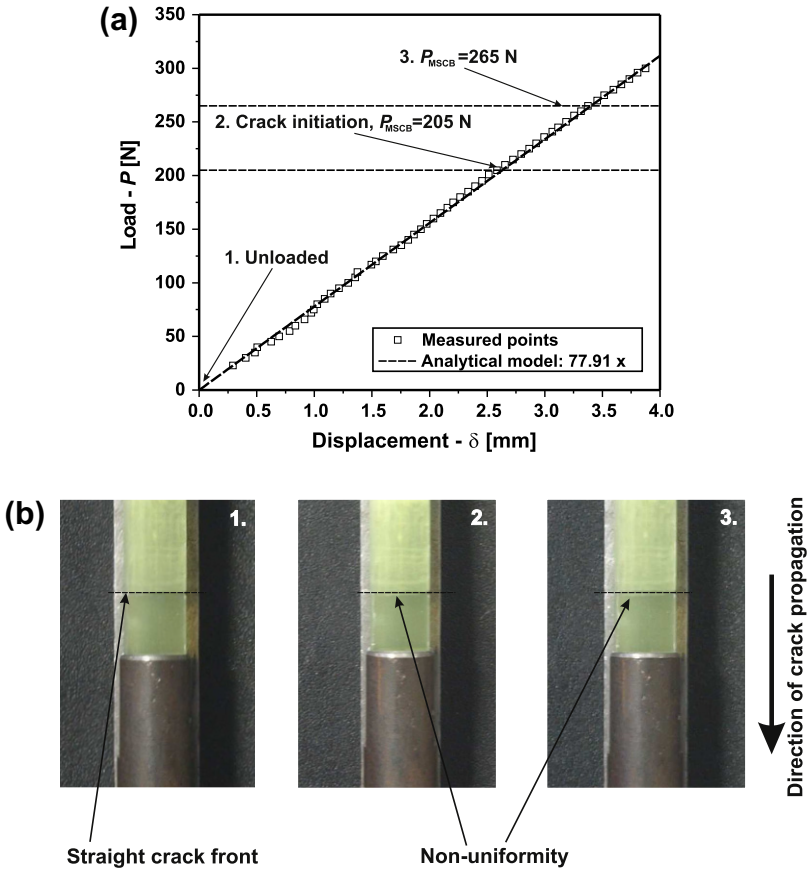

Fig. 9. The load–displacement curve of the $PSCB_{II/III}$ system for δ_{ELS} = 11.375 mm (a). The identification of crack initiation during the fracture process (b). (For interpretation of the references to colour in this figure legend, the reader is referred to the web version of this article.)

Table 1
The changes in the slope of the load displacement curves of the $PSCB_{II/III}$ specimen with the prestressing displacement.

δ_{ELS} (mm)	0(MSCB)	4.6875	6.25	8.125	9.375	10.625	11.875	13.75
Load–displacement curve slope-1 (N/mm)	77.429[a]	77.31	75.93	78.09	79.31	77.47	79.11	83.84
Difference compared to 77.91 (N/mm)[b]	5.60[a]	−0.77	−2.54	0.23	1.80	−0.56	1.54	7.61
Load–displacement curve slope-2 (N/mm)	75.74[a]	75.31	76.84	79.57	76.93	80.27	76.92	72.28
Difference compared to 77.91 (N/mm)[b]	3.30[a]	−3.34	−1.37	2.13	−1.26	3.03	−1.27	−7.23

[a] s_1 = 49.25 mm, s_2 = 51.15 mm.
[b] Result of the analytical model.

To evaluate the test results the mode-I, mode-II and mode-III ERRs are calculated by the VCCT and at each point the total ERR and the mode ratio are also determined. In the sequel the details of the experimental work is presented.

4. Experiments

4.1. Material properties

The details of the specimen preparation and the determination of the material properties of the unidirectional E-glass/polyester composite material was presented in several other papers [19,22].

4.2. End-loaded split test

In the case of the ELS test (Fig. 1b) we refer to previous fracture experiments [32] performed for a = 105 mm. Four specimens was tested and it has been found that the initiation ERR was G_{IIC} = 768 J/m^2 evaluated by using the VCCT. The width of the specimens was b = 20 mm.

4.3. Modified split-cantilever beam test

For the MSCB measurements four specimens were prepared with a = 105 mm, b = 12.8 mm and s_1 = 49.25 mm, s_2 = 51.15 mm, respectively. Each specimen was put into the loading rig shown in Fig. 1 (or detailed in [19]), the rig was adjusted in order to eliminate any play of the specimens. Then the specimens were tested, the load and displacement values were read from the scale of the testing machine and using a digitronic indicator. The crack initiation was identified by naked eye and when the first non-uniformity in the previously straight crack front was observed it was believed to be the point of crack initiation (see Fig. 8). The initation ERR was G_{IIIC} = 139 J/m^2.

This value is significantly less than G_{IIC}, and in general the mode-III ERR is expected to be higher than G_{IIC}. It should be mentioned that in [22] for the same material G_{IIIC} = 446 J/m^2 was obtained. However, in the latter paper the utilized MSCB fixture was not the same as the one shown in Figs. 1 and 8. The rigs were connected to each other by screws, which induced friction between them. Probably, this effect caused the mentioned difference. On the

Please cite this article in press as: Szekrényes A, Vicente WM. Interlaminar fracture analysis in the G_{II}–G_{III} plane using prestressed transparent composite beams. Composites: Part A (2011), doi:10.1016/j.compositesa.2011.09.022

other hand the crack length of interest was $a = 55$ mm in [22], in contrast with the current tests, where we applied specimens with $a = 105$ mm. A certain dependence on the crack length can exist [30]. In general, the mode-III toughness for glass fiber-reinforced composites reported in the literature is much higher [10,33,34] (1200–3000 J/m^2) than the value obtained in this paper. Nevertheless, the former works presented ECT test results with multidirectional lay-ups, while the present test applied unidirectional beam-like samples.

4.4. Prestressed split-cantilever beam test

The PSCB$_{II/III}$ test setup is presented in Fig. 8. The tests were carried out using an Amsler testing machine under displacement control, the specimen displacement was recorded by a digitronic indicator. The crack length of interest was $a = 105$ mm, the width of the specimens was $b = 12.8$ mm. The critical specimen end displacement measured from the ELS test [32] is about 14 mm (if $a = 105$ mm and $L = 118$ mm). According to this fact, six different values of the ELS displacement δ_{ELS} were set: 4.6875, 6.25, 8.125, 9.375, 10.625 and 11.875 mm. The setup and the concept of the system is shown in Fig. 1. Similarly to the MSCB tests, we applied four coupons at each displacement value. The load–deflection data was measured by using the scale of the testing machine and a digitronic indicator. In each case the critical load at crack initiation was determined.

5. Results and discussion

It will be shown subsequently that the stiffness and the compliance of the PSCB$_{II/III}$ specimen are identical (with a very good approximation) to those of the MSCB specimen.

5.1. Load and displacement

Fig. 9a shows a recorded load–displacement trace for the *PSCB*$_{II/III}$ specimen if $\delta_{ELS} = 11.875$ mm. The response follows essentially a linear relation. The PSCB$_{II/III}$ test was performed according to the followings. The onset of crack advance was identified by visual observations. It was found that crack initiation was the primary damage mode and no other damage prior (or simultaneously) to delamination initiation was observed. In each case four specimens were tested, one of them was used to investigate the crack front. The other three specimens were loaded continuously and the crack initiation was observed in situ. Accordingly, the former specimen was loaded subsequently, at some points, where the initiation was expected the specimen was relieved, removed from the rig and the crack front was photographed. When the first non-uniformity was observed, then this point was denoted to be the point of fracture initiation. The results of this process are demonstrated in Fig. 9b for the PSCB$_{II/III}$ system at a prestressed state with $\delta_{ELS} = 11.875$ mm.

Also, the crack initiation point in Fig. 9b agrees very well with the G_{Tmax} point indicated in Fig. 7.

Table 1 shows that the slopes of the load–displacement traces of the MSCB ($\delta_{ELS} = 0$) and PSCB$_{II/III}$ specimens are eventually the same, consequently the prestressed state does not influence noticeably the stiffness of the system and the compliance of the PSCB$_{II/III}$ can be assumed to be equal to that of the MSCB system. The maximum difference is 7.6% between the measured and calculated slopes.

5.2. Fracture envelopes

The critical mode-II, mode-III and the mixed-mode II/III ERRs at crack initiation and the mode mix were calculated by the VCCT. The point of crack initiation was believed to be the point where the highest ERR was available. Accordingly, using the distributions depicted by Fig. 7 the critical ERRs and the mode ratio were obtained for each prestressed state. We note again that Eq. (7) was violated, however this can be corrected by changing the divisions of the holes for the loading pins. Also, it is assumed, that due to the small displacements of the ELS part, and the small diameter of the set screw (4 mm), there is no need to correct the crack length of the specimen. Based on the nature of the reduced G_{II}–G_{III} data the so-called power criterion and the one developed by Williams are applied to construct the fracture envelope in the G_{II}–G_{III} plane. The power criterion is [35]:

$$\left(\frac{G_{III}}{G_{IIIC}}\right)^{p_1} + \left(\frac{G_{II}}{G_{IIC}}\right)^{p_2} = 1. \tag{8}$$

Williams' criterion is [25]:

$$\frac{G_{II}}{G_{IIC}} + \frac{G_{III}}{G_{IIIC}} + (I_{23} - 1)\left(\frac{G_{II}}{G_{IIC}}\right)\left(\frac{G_{III}}{G_{IIIC}}\right) = 1. \tag{9}$$

In Eqs. (8) and (9) G_{IIC} is the critical ERR under pure mode-II (calculated from the data of the ELS specimen), G_{IIIC} is the mode-III critical ERR (calculated from the data of the MSCB specimen). The results of the PSCB$_{I/III}$ test were used to provide six additional points in the G_{II}–G_{III} plane. The power parameters in Eq. (8), the interaction parameter and the fracture envelope was calculated in the code ORIGIN 8.0. The fracture envelopes are displayed in Fig. 10. The shape of the curve is convex, in contrast with some previous results [27,32]. The main conclusion is that there is a significant interaction between the mode-II and mode-III ERRs.

It is important to note that by knowing the critical ERRs (G_{IIC}, G_{IIIC}) and the interaction parameter, I_{23} it is possible to apply Eqs. (8) and (9) in the other points along the crack front. As Table 2 shows in this case it is possible that we obtain a number higher than unity in the right-hand side of Eqs. (8) and (9), which means seemingly that there are more dangerous points apart from the point of crack initiation. However, it is important that Eqs. (8) and (9) assume crack initiation, which was detected only at one point, namely, where G_T was maximal (refer to Fig. 7). Therefore, the other points, where Eqs. (8) and (9) give >1 should be ignored.

In some recent works the fracture envelopes in the G_I–G_{II} and G_I–G_{III} planes were constructed by the mixed-mode I/II PELS and the mixed-mode I/III version of the PSCB specimen (PELS$_{I/II}$ and PSCB$_{I/III}$) for the same E-glass/polyester material [25,32] resulting in a concave envelope in the G_I–G_{II} and even a concave one in the G_{II}–G_{III} plane (see Fig. 11). It is important to highlight that the

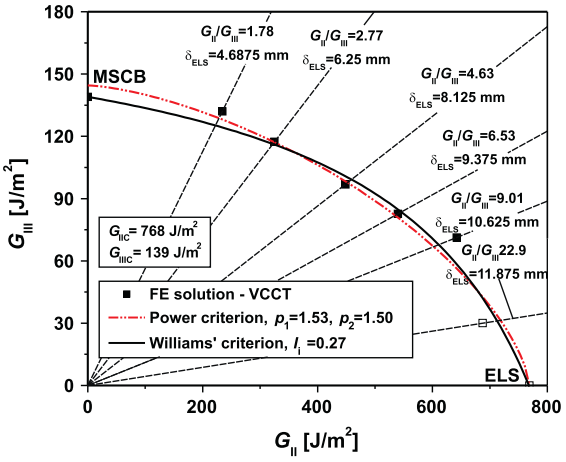

Fig. 10. Interlaminar fracture envelopes in the G_{II}–G_{III} plane for E-glass/polyester composite material determined by the VCCT method. (For interpretation of the references to colour in this figure legend, the reader is referred to the web version of this article.)

Please cite this article in press as: Szekrényes A, Vicente WM. Interlaminar fracture analysis in the G_{II}–G_{III} plane using prestressed transparent composite beams. Composites: Part A (2011), doi:10.1016/j.compositesa.2011.09.022

Table 2
The results of the fracture criterion (Eq. (9)) at the points of the crack front for the $PSCB_{II/III}$ specimen, δ_{ELS} = 9.375 mm, P_{MSCB} = 297.5 N.

z – Distance from the edge of delamination front (mm)	0.00	1.28	2.56	3.84	5.12	6.40	7.68	8.96	10.24	11.52	12.80
Criterion – Eq. (9)	0.62	1.12	1.18	1.20	1.19	1.16	1.12	1.07	0.99[a]	0.84	0.24

[a] Point of crack initiation

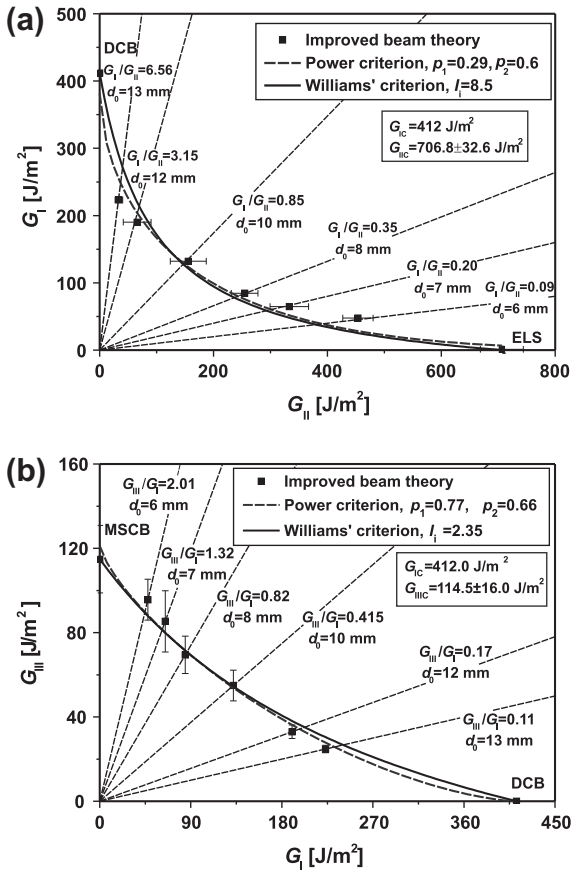

Fig. 11. Interlaminar fracture envelopes in the G_I–G_{II} and G_I–G_{III} planes for E-glass/polyester composite material determined by the improved beam theory (IBT).

envelopes in Fig. 11 are calculated based on the IBT scheme, which reflects the widthwise average of the ERRs. Under mixed-mode I/II and I/III the ERR distributions are symmetric with respect to the specimen width. In contrast, the joint presence of the mode-II and mode-III ERRs leads to the asymmetric distributions presented in Fig. 7.

Although a somewhat different data reduction was applied, based on the comparison between Fig. 10 and the envelopes given by Fig. 11 we may conclude that the material behaves differently under mixed-mode II/III than under mixed-mode I/II and I/III loading conditions, but proves similar behavior in the G_I–G_{II}, and the G_I–G_{III} planes. It is also important to note that interaction takes place in each case.

6. Conclusions

In this work the mixed-mode II/III version of the prestressed split-cantilever beam specimen was developed for interlaminar fracture testing of laminated transparent composite materials. Apart from the MSCB and the traditional ELS tests, the $PSCB_{II/III}$ specimen was used to obtain the mixed-mode II/III ERR at crack propagation onset including six different mode ratios. To perform the experiments unidirectional E-glass/polyester specimens were manufactured. FE analysis was performed and it was shown that the mode ratio changes significantly along the specimen width and it is not possible to eliminate this variation. The crack initiation was expected at the point where the maximum of the total ERR was calculated. Based on the performed experimental work the fracture envelope of the present material was determined indicating significant interaction between G_{II} and G_{III}.

One of the advantages of the $PSCB_{II/III}$ specimen is that it incorporates the traditional beam-like specimen geometry. Although the experiments were performed on unidirectional samples, it is possible to test specimens with other, symmetric lay-ups. Second, it was shown that the $PSCB_{II/III}$ specimen is able to produce any mode ratio at crack propagation onset. Further drawback is that the mode ratio changes with the crack length and the applied load, so the method is recommended mainly for the testing of transparent composite materials. Moreover the mode ratio changes significantly along the crack front. Also, the mode ratio can not be calculated without performing experiments, involving the fact that the mode ratio will depend on the definition of the crack initiation and the accuracy of the measurement of the load and crack length.

More research is needed to reduce the drawbacks of the test and to make it possible to test non-transparent materials.

Acknowledgments

This paper was supported by the János Bolyai Research Scholarship of the Hungarian Academy of Sciences and the National Science and Research Fund (OTKA) under Grant No. T34040 (69096). This work is connected to the scientific program of the "Development of quality-oriented and harmonized R+D+I strategy and functional model at BME" project. This project is supported by the New Hungary Development Plan (Project ID: TÁMOP-4.2.1/B-09/1/KMR-2010-0002). The first author is grateful to his father (András L. Szekrényes) for the construction of the experimental equipment.

References

[1] Brunner AJ, Flüeler P. Prospects in fracture mechanics of "engineering" laminates. Eng Fract Mech 2005;72:899–908.
[2] Brunner AJ, Blackman BRK, Davies P. A status report on delamination resistance testing of polymer–matrix. Eng Fract Mech 2008;75:2779–94.
[3] ASTM D6671/D6671M-06 standard test method for mixed mode I–mode II interlaminar fracture toughness of unidirectional; 2006.
[4] Determination of the mixed-mode I/II delamination resistance of unidirectional fibre-reinforced polymer laminates using the asymmetric double cantilever beam specimen (ADCB). European Structural Integrity Society (ESIS), Polymers and Composites Task Group; version 00-05-03 ed.; 2000.
[5] Becht Jr G, Gillepie JWG. Design and analysis of the crack rail shear specimen for mode III interlaminar fracture. Compos Sci Technol 1988;31:143–57.
[6] Donaldson SL. Mode III interlaminar fracture characterization of composite materials. Compos Sci Technol 1988;32:225–49.
[7] Lee SM. An edge crack torsion method for mode III delamination fracture testing. J Compos Technol Res 1993;15(3):193–201.
[8] Liao WC, Sun CT. The determination of mode III fracture toughness in thick composite laminates. Compos Sci Technol 1996;56:489–99.
[9] Ratcliffe JG. Characterization of the edge crack torsion (ECT) test for mode III fracture toughness measurement of laminated composites. Technical Memorandum 213269, NASA; 2004.
[10] Pennas D, Cantwell WJ, Compston P. The influence of strain rate on the mode III interlaminar fracture of composite materials. J Compos Mater 2007;41:2395–614.

[11] de Morais AB, Pereira AB, de Moura MFSF, Magalhães AG. Mode III interlaminar fracture of carbon/epoxy laminates using the edge crack torsion (ECT) test. Compos Sci Technol 2009;69:670–6.
[12] Robinson P, Song QD. The development of an improved mode III delamination test for composites. Compos Sci Technol 1994;52:217–33.
[13] Cicci D, Sharif F, Kortschot MT. Data reduction for the split cantilever beam mode III delamination test. In: Proceedings, ACCM 10. Whistler, British Columbia, Canada; 1995. p. 1–8.
[14] Trakas K, Kortschot MT. The relationship between critical strain energy release rate and fracture mode in multidirectional carbon-fiber/epoxy laminates. In: Armanios A, editor. Composite materials: fatigue and fracture – sixth volume, vol. ASTM STP 1285. ASTM; 1997. p. 283–304.
[15] Rizov V, Shindo Y, K KH, Narita F. Mode III interlaminar fracture behaviour of glass fiber reinforced polymer woven laminates at 293 to 4 K. Appl Compos Mater 2006;13:287–304.
[16] Farshad M, Flüeler P. Investigation of mode III fracture toughness using an anti-clastic plate bending method. Eng Fract Mech 1998;60:5–6.
[17] Yoshihara H. Examination of the 4-ENF test for measuring the mode III *R*-curve of wood. Eng Fract Mech 2006;73:42–63.
[18] de Morais AB, Pereira AB. Mode III interlaminar fracture of carbon/epoxy laminates using a four-point bending plate test. Compos Part A – Appl Sci Manuf 2009;40(11):1741–6.
[19] Szekrényes A. Improved analysis of the modified split-cantilever beam for mode-III fracture. Int J Mech Sci 2009;51:682–93.
[20] Pereira AB, de Morais AB, de Moura MFSF. Design and analysis of a new six-point edge crack torsion (6ECT) specimen for mode III interlaminar fracture characterisation. Compos Part A – Appl Sci Manuf 2011;42(2):131–9.
[21] Davidson BD, Sediles FO. Mixed-mode I–II–III delamination toughness determination via a shear torsion-bending test. Composites: Part A 2011;42:589–603.
[22] Szekrényes A. Delamination fracture analysis in the G_{II}–G_{III} plane using prestressed transparent composite beams. Int J Solids Struct 2007;44:3359–78.
[23] Pereira AB, de Morais AB. Mixed mode I + III interlaminar fracture of carbon/epoxy laminates. Compos Part A – Appl Sci Manuf 2009;40(4):518–23.
[24] de Morais AB, Pereira AB. Mixed mode II + III interlaminar fracture of carbon/epoxy laminates. Compos Part A – Appl Sci Manuf 2008;68(9):2022–7.
[25] Szekrényes A. Interlaminar fracture analysis in the G_I–G_{III} plane using prestressed transparent composite beams. Compos Part A – Appl Sci Manuf 2009;40(10):1621–31.
[26] Suemasu H, Kondo A, Gozu K, Aoki Y. Novel test method for mixed mode II and III interlaminar fracture toughness. Adv Compos Mater 2010;19:349–61.
[27] Szekrényes A. Prestressed fracture specimen for delamination testing of composites. Int J Fract 2006;139:213–37.
[28] Szekrényes A. Improved analysis of unidirectional composite delamination specimens. Mech Mater 2007;39:953–74.
[29] Sharif F, Kortschot MT, Martin RH. Mode III delamination using a split cantilever beam. In: Martin RH, editor. Composite materials: fatigue and fracture – fifth volume, vol. ASTM STP 1230. Philadelphia: ASTM; 1995, p. 85–99.
[30] Szekrényes A. The influence of crack length and delamination width on the mode-III energy release rate of laminated composites. J Compos Mater 2011;59(3).
[31] Polaha J, Davidson B, Hudson R, Pieracci A. Effects of mode ratio, ply orientation and precracking on the delamination toughness of a laminated composite. J Reinf Plast Compos 1996;15:141–73.
[32] Szekrényes A. Prestressed composite specimen for mixed-mode I/II cracking in laminated materials. J Reinf Plast Compos 2010;29:3309–21.
[33] Li X, Carlsson L, Davies P. Influence of fiber volume fraction on mode III interlaminar fracture toughness of glass/epoxy composites. Compos Sci Technol 2004;64:1279–86.
[34] Marat-Mendes RM, Freitas MM. Failure criteria for mixed mode delamination in glass fibre epoxy composites. Compos Struct 2010;92(9):2292–8.
[35] Reeder JR. An evaluation of mixed-mode delamination failure criteria. Technical Memorandum 104210, NASA; 1992.

Please cite this article in press as: Szekrényes A, Vicente WM. Interlaminar fracture analysis in the G_{II}–G_{III} plane using prestressed transparent composite beams. Composites: Part A (2011), doi:10.1016/j.compositesa.2011.09.022